pubs.acs.org/Biomac

Article

ROS-Responsive Selenopolypeptide Micelles: Preparation, Characterization, and Controlled Drug Release

Chenglong Ge,[§] Junliang Zhu,[§] Guangqi Wu, Huan Ye, Hua Lu,* and Lichen Yin*

Cite This: *Biomacromolecules* 2022, 23, 2647−2654

Read Online

ACCESS | Metrics & More | Article Recommendations | Supporting Information

ABSTRACT: Sulfur-containing polypeptides, capable of reactive oxygen species (ROS)-responsive structural change, are one of the most important building blocks for the construction of polypeptide-based drug delivery systems. However, the relatively low ROS sensitivity of side-chain thioethers limits the biomedical applications of these polypeptides because they usually require a high concentration of ROS beyond the pathological ROS level in the tumor microenvironment. Herein, we report the design and synthesis of a selenium-containing polypeptide, which undergoes random coil-to-extended helix and hydrophobic-to-hydrophilic transitions in the presence of 0.1% H_2O_2, a concentration that is much lower than the ROS requirement for thioether. ROS-responsive micelles were thus prepared from the amphiphilic copolymer consisting of the hydrophilic poly(ethylene glycol) (PEG) segment and hydrophobic selenopolypeptide segment and were used to encapsulate doxorubicin (DOX). The micelles could be sensitively dissociated inside tumor cells in consequence of ROS-triggered oxidation of side-chain selenoether and structural change of the micelles, thereby efficiently and selectively releasing the encapsulated DOX to kill cancer cells. This work provides an alternative design of ROS-responsive polypeptides with higher sensitivity than that of the existing sulfur-containing polypeptides, which may expand the biomedical applications of polypeptide materials.

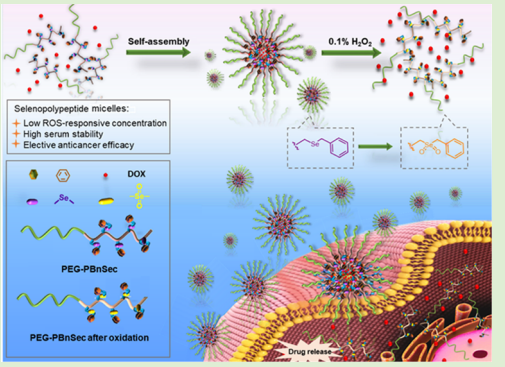

INTRODUCTION

Polypeptides are synthetic analogues of natural proteins with excellent biocompatibility and biodegradability and have shown wide utilities in the biomedical field. Amphiphilic, polypeptide-based diblock copolymers, such as poly(ethylene glycol) (PEG)-*block*-polypeptides, can self-assemble into nanostructures that serve as promising vehicles for drug delivery.[1−11] The versatile side chain design of synthetic polypeptides allows facile incorporation of trigger-responsive moieties, which enable controlled release of encapsulated cargos from polypeptide-based nanocarriers.[12−14] Additionally, polypeptides adopt unique secondary structures, such as α-helix and β-sheet, which are also closely associated with the structure and function of polypeptide-based nanovehicles.[15−17] Sulfur-containing polypeptides, including those with disulfide and thioether side chains, are widely studied as the building blocks of polypeptide-based nanoassemblies, mainly due to their redox responsiveness that triggers the structural change of the nanocarriers and subsequently promotes the release of cargos.[18−24] Specifically, thioethers on polypeptide side chains can be oxidized to sulfoxide or sulfone groups by reactive oxygen species (ROS), resulting in significant changes in the side-chain polarity, hydrophilicity, and even the backbone secondary structure.[25] As a result, amphiphilic block copolymer assemblies based on thioether-containing polypeptides can experience ROS-responsive structural change and subsequently lead to the release of the encapsulated payloads.[26−30] Nevertheless, oxidation of thioether usually requires a relatively high concentration of ROS (typically 10% H_2O_2, v/v),[31] which greatly limits its application in the *in vivo* environment.

Selenium is an essential element in the human body, and one of its important functions is to regulate the oxidation balance in the organism.[32] Compared with sulfur, selenium possesses higher reactivity due to its lower electronegativity and larger atomic radius.[33] Particularly, selenoether can be oxidized to selenosulfone using 0.1% H_2O_2, a much milder oxidation condition than that required for the oxidation of thioether.[34,35] Thus, nanodelivery systems based on amphiphilic, selenium-containing polymers have been widely developed, which exhibit higher ROS responsiveness than that of sulfur-containing polymers to enable on-demand drug release in tumor cells with overproduced ROS.[36−41] Selenium-containing polypeptides have also been studied in recent years, focusing on the oxidation-triggered conformational transition and the protection of functional proteins against oxidative

Received: March 30, 2022
Revised: April 27, 2022
Published: May 12, 2022

https://doi.org/10.1021/acs.biomac.2c00399
Biomacromolecules 2022, 23, 2647−2654

Scheme 1. Illustration of the Formation of Selenium-Containing Polypeptide Micelles and Their ROS-Responsive Drug Release Behavior in Cancer Cells

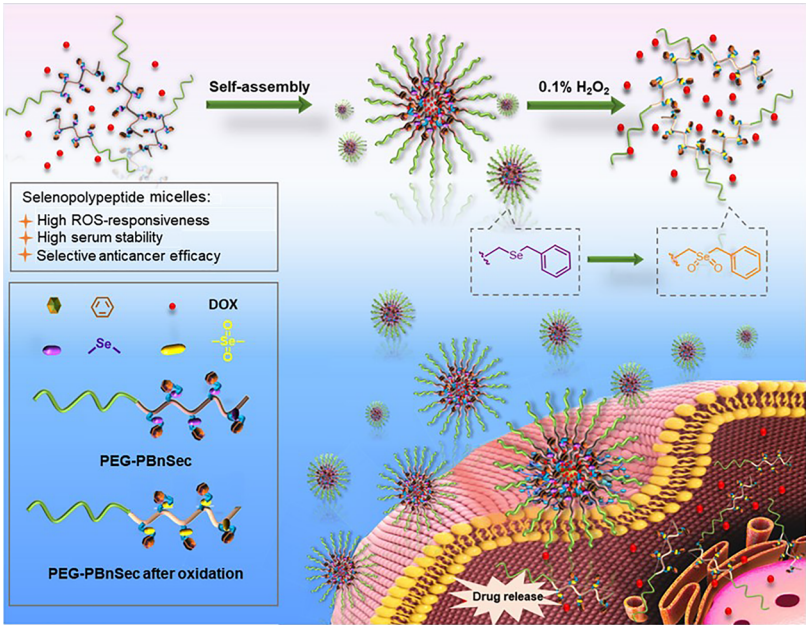

stress.[42−44] Nonetheless, the use of selenium-containing polypeptides as ROS-responsive nanovehicles for drug delivery has not been carefully studied.

Herein, we report the development of ROS-responsive micelles based on PEG-*block*-poly(*Se*-benzyl-L-selenocysteine) (PEG-PBnSec), an amphiphilic copolymer with selenium-containing polypeptide as the hydrophobic block. The selenoether on the polypeptide side chain could be sensitively oxidized by overproduced H_2O_2 in cancer cells, leading to the hydrophobic-to-hydrophilic and random coil-to-extended helix transitions of the PBnSec segment. Such transitions then propelled the structural change of micelles and release of the encapsulated chemodrug, doxorubicin (DOX), thereby inducing selective killing of cancer cells (Scheme 1). Based on the high ROS responsiveness and excellent biocompatibility of the selenopolypeptide micelles, we believe that our work may expand the design of smart, trigger-responsive polypeptide biomaterials.

EXPERIMENTAL SECTION

Synthesis of *N*-(*tert*-Butoxycarbonyl)-L-Diselenocysteine Methyl Ester (Boc-DiSec-OMe). $NaBH_4$ (102 mg, 2.68 mmol) was dissolved in deionized (DI) water (5 mL), into which selenium powder (212 mg, 2.68 mmol) was added. The resulting mixture was stirred at 50 °C for 20 min in a nitrogen atmosphere. A solution of Boc-Ser(Tos)-OMe (1.0 g, 2.68 mmol) in acetonitrile (5 mL) was added, and the mixture was stirred at 50 °C for 5 h in a nitrogen atmosphere. After removal of acetonitrile under vacuum, the mixture was dispersed in the aqueous solution of saturated NaCl (20 mL) and extracted with dichloromethane (DCM) (30 mL × 5). The organic layer was dried over anhydrous Na_2SO_4 at 0 °C. The crude product was obtained after evaporation of the solvent, and it was further purified by extraction with diethyl ether to remove the insoluble impurities. Boc-DiSec-OMe was thus obtained as a yellow viscous liquid (0.49 g, 65% yield).

Synthesis of *N*-(*tert*-Butoxycarbonyl)-*Se*-Benzyl-L-Selenocysteine Methyl Ester (Boc-Bn-Sec-OMe). Boc-DiSec-OMe (0.49 g, 0.87 mmol) and benzyl bromide (0.33 g, 1.92 mmol) were dissolved in tetrahydrofuran (THF) (5 mL) in a nitrogen atmosphere. A freshly prepared aqueous solution (1.46 mL) of $NaBH_4$ (66 mg, 1.74 mmol) and NaOH (3.5 mg, 0.087 mmol) was added. The mixture was stirred at room temperature for 5 h. The solvent was removed under vacuum, and the resulting mixture was dispersed in the aqueous solution of saturated NaCl (15 mL) and HCl (1 M, 15 mL), which was extracted with DCM (30 mL × 5). The organic layer was dried over anhydrous Na_2SO_4 at 0 °C. Boc-Bn-Sec-OMe was obtained as a light-yellow viscous liquid after removal of the solvent under vacuum (0.57 g, 87% yield).

Synthesis of *Se*-Benzyl-L-Selenocysteine (Bn-Sec). Boc-Bn-Sec-OMe (0.57 g, 1.53 mmol) was dissolved in DCM (10.3 mL) in an ice−water bath, into which a solution of DCM/trifluoroacetic acid (10.3 mL, 4:1, v/v) was slowly added. The mixture was stirred at room temperature for 3 h, and *Se*-benzyl-L-selenocysteine methyl ester (Bn-Sec-OMe) was obtained as a light-yellow liquid after removal of the solvent under vacuum. The obtained Bn-Sec-OMe was directly mixed with HCl (6 M, 4 mL) in a nitrogen atmosphere, which was stirred at 75 °C for 12 h. After removal of the solvent under vacuum, the crude product was washed with diethyl ether for three times to obtain Bn-Sec as a white solid (0.29 g, 74% yield).

Synthesis of *Se*-Benzyl-L-Selenocysteine *N*-Carboxyanhydride (Bn-Sec-NCA). Triphosgene (0.23 g, 0.749 mmol), Bn-Sec (0.29 g, 1.12 mmol), and anhydrous THF (10 mL) were mixed in a round-bottom flask in a nitrogen atmosphere. The mixture was stirred at 50 °C for 24 h. The insoluble substance was removed via filtration, and the solvent was removed under vacuum, yielding a brown viscous liquid, which was purified by silica gel chromatography with ethyl acetate as the eluent. Finally, the product was recrystallized in ethyl acetate/hexane (1:10, v/v) at −20 °C for three times to afford Bn-Sec-NCA as a white solid (0.25 g, 78% yield).

Synthesis of PEG-PBnSec. In a glovebox, Bn-Sec-NCA (62 mg, 0.22 mmol) was dissolved in anhydrous *N*,*N*-dimethylformamide (DMF) (2 mL), into which a solution of mPEG-NH_2 (72 mg, 0.014 mmol, $[M]_0/[I]_0$ = 15) in DMF (0.5 mL) was added. The reaction mixture was stirred at room temperature for 72 h. The product was purified by dialysis against DI water (molecular weight cutoff (MWCO) = 3.5 kDa) for 3 days followed by lyophilization, which yielded PEG-PBnSec as a white solid (61 mg, 69% yield).

Preparation and Characterization of PEG-PBnSec and PEG-PBnSec/DOX Micelles. PEG-PBnSec micelles were prepared by the nanoprecipitation method.[45−47] Specifically, DMF solution of PEG-PBnSec (0.5 mL, 10 mg/mL) was added dropwise into DI water (4.5 mL) under vigorous stirring. The mixture was stirred at room

https://doi.org/10.1021/acs.biomac.2c00399
Biomacromolecules 2022, 23, 2647−2654

Scheme 2. Synthetic Routes to the Amphiphilic Diblock Copolymer PEG-PBnSec Bearing a Selenium-Containing Polypeptide Segment

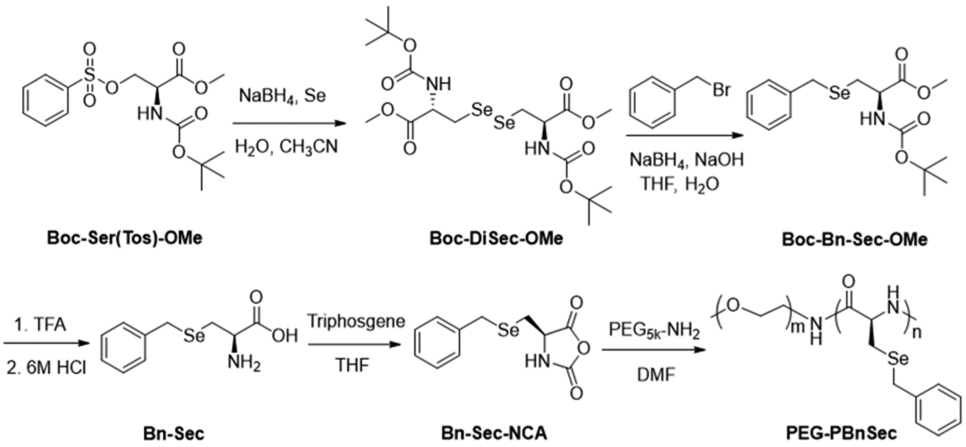

temperature for 6 h. DMF was removed by dialysis (MWCO = 3.5 kDa) against DI water for 24 h. The particle size of the obtained micelles was then measured by dynamic light scattering (DLS). The morphology of the micelles was observed by transmission electron microscopy (TEM) according to the reported method.[48]

Drug-loaded PEG-PBnSec micelles were prepared by the same method using DOX as a model chemotherapeutic agent.[45−47] The detailed preparation process and the determination of drug loading content (DLC) and drug loading efficiency (DLE) are described in the Supporting Information.

ROS Responsiveness of PEG-PBnSec Micelles. PEG-PBnSec micelles (10 mg/mL, 0.5 mL) were mixed with 0.1% H_2O_2 (10 mL) and incubated at 37 °C. The particle size of the micelles was measured by DLS at predetermined time intervals (0, 2, 4, 8, 12, and 24 h) to evaluate the stability against ROS. To further characterize the chemical structures of micelles after oxidation, PEG-PBnSec micelles (10 mg/mL, 1 mL) were treated with 0.1% H_2O_2 (20 mL) for 16 h, dialyzed (MWCO = 3.5 kDa) against DI water for 3 days, and lyophilized to afford a white solid. The structures of micelles after oxidation were characterized by proton nuclear magnetic resonance (^{1}H NMR), circular dichroism (CD), and Fourier transform infrared (FT-IR) as described above. In addition, the ROS-responsive drug release profile from DOX-loaded PEG-PBnSec micelles was further studied according to the previous literature,[45−47,49,50] and the details are described in the Supporting Information.

***In Vitro* Cell Uptake and Intracellular Distribution.** HeLa, HepG2, 4T1, H9C2, or 3T3 cells were seeded on the coverslips in 6-well plates at 1 × 10^5 cells/well and cultured for 24 h. After replacement with fresh medium containing 10% fetal bovine serum (FBS) (2 mL), PEG-PBnSec/DOX micelles were added at the final DOX concentration of 5 μg/mL and incubated with cells for 6 h at 37 °C. Cells were washed with cold phosphate-buffered saline (PBS) for three times, fixed with 4% paraformaldehyde for 15 min, stained with 4′,6-diamidino-2-phenylindole (DAPI) (5 μg/mL, 8 min) for the nuclei, and then visualized by confocal laser scanning microscopy (CLSM). To further probe the ROS responsiveness of PEG-PBnSec/DOX micelles, 3T3 cells were incubated with PEG-PBnSec/DOX micelles in fresh Dulbecco's modified Eagle medium (DMEM) (2 mL, containing 0.1% H_2O_2 and 10% FBS) for 6 h at the final DOX concentration of 5 μg/mL. Cells were treated by the same method as described above and then visualized by CLSM.

HeLa and 3T3 cells were seeded on 6-well plates at 1 × 10^5 cells/well and cultured for 24 h. After replacement with fresh DMEM containing 10% FBS (2 mL), PEG-PBnSec/DOX micelles were added at the final concentration of 5 μg DOX/mL and incubated with cells for 6 h at 37 °C. Then, cells were washed with cold PBS for three times and lysed with the RIPA lysis buffer (1 mL/well). The protein level in the lysate was quantified using the bicinchoninic acid (BCA) kit. The lysate was further one-fold diluted with DMF, and the DOX amount in the lysate was determined by spectrofluorimetry (λ_{ex} = 480 nm, λ_{em} = 590 nm). Finally, the cellular uptake level was expressed as μg of DOX associated with 1 mg of protein.

***In Vitro* Anticancer Efficacy.** The *in vitro* anticancer efficacy of PEG-PBnSec/DOX micelles was evaluated by the 3-[4,5-dimethylthiazol-2-yl]-2,5- diphenyl tetrazolium bromide (MTT) assay. Briefly, HeLa, HepG2, 4T1, H9C2, or 3T3 cells were seeded on 96-well plates at 7 × 10^3 cells/well and incubated at 37 °C for 24 h. After replacement with fresh medium containing 10% FBS, free DOX or PEG-PBnSec/DOX micelles were added at different final concentrations of DOX. After 48 h of incubation, the cell viability was measured by the MTT assay. Results were presented as percentage viability of control cells that did not receive treatment with free DOX or PEG-PBnSec/DOX micelles.

RESULTS AND DISCUSSION

Synthesis and Characterization of PEG-PBnSec. To obtain the selenium-containing polypeptide, *Se*-benzyl-L-selenocysteine (Bn-Sec) was first synthesized through three steps (Scheme 2). First, the diselenide group was introduced onto the side chain of amino acid through the reaction between selenium powder and *N*-boc-*O*-(4-toluenesulfonyl)-L-serine methyl ester (Boc-Ser(Tos)-OMe). Matrix-assisted laser desorption/ionization time of flight mass spectrometry (MALDI-TOF MS) confirmed the structure of the target product, as characterized by a series of molecular ion peaks at m/z ∼ 585 ([M + Na]$^+$ species) that corresponded to the multiple isotopes of the selenium element (Figure S1). Compared with the ^{1}H NMR spectrum of the starting amino acid, the disappearance of aromatic protons at 7.32 and 7.88 ppm and the upfield shift of β-protons (from 4.30−4.50 to 3.30−3.50 ppm) in the ^{1}H NMR spectrum of the product also indicated the successful reaction (Figure S2). In the second step, the diselenide group was transformed into the selenoether group through reduction and subsequent nucleophilic reaction with benzyl bromide, leading to the formation of *N*-(*tert*-butoxycarbonyl)-*Se*-benzyl-L-selenocysteine methyl ester (Boc-Bn-Sec-OMe). Finally, the removal of Boc and methyl protecting groups generated the target product Bn-Sec that was used for *N*-carboxyanhydride (NCA) preparation. The successful synthesis of Bn-Sec was verified by ^{1}H NMR, which showed the appearance of aromatic protons (7.28 ppm) and the disappearance of protons from the protecting groups (1.45 and 3.72 ppm for Boc and methyl groups, respectively) (Figures S3 and S4).

https://doi.org/10.1021/acs.biomac.2c00399
Biomacromolecules 2022, 23, 2647−2654

The obtained Bn-Sec was treated with triphosgene, yielding *Se*-benzyl-L-selenocysteine NCA (Bn-Sec-NCA). The appearance of the characteristic peak at 6.12 ppm in the ^{1}H NMR spectrum, attributed to the ring N−H group of the NCA monomer, verified the successful ring closing reaction (Figure S5). Additionally, new bands at 1835 and 1782 cm^{-1} in the FT-IR spectrum, corresponding to the anhydride moieties, further validated the successful preparation of the Bn-Sec-NCA monomer (Figure S6).

The ring-opening polymerization (ROP) of Bn-Sec-NCA was then conducted using mPEG-NH_2 as the macroinitiator ($[M]_0/[I]_0$ = 15). The disappearance of anhydride peaks in the FT-IR spectrum indicated successful polymerization (Figure S6), and ^{1}H NMR verified the structure of the obtained PEG-PBnSec (Figure S7). Gel permeation chromatography (GPC) analysis further demonstrated the successful ROP initiated by mPEG-NH_2, with a clear peak shift to the higher molecular weight (MW) region (M_n = 8.6 kDa, DP = 15, $Đ$ = 1.24) (Figure S8). The shoulder peak on the GPC trace likely came from the dimeric impurity in the mPEG-NH_2 initiator, which led to uncontrolled polymerization.[51]

Characterization of PEG-PBnSec Micelles. The amphiphilic diblock copolymer PEG-PBnSec self-assembled into micelles with a hydrophilic PEG shell and a hydrophobic PBnSec core. The critical micelle concentration (CMC) of PEG-PBnSec at room temperature was determined to be 3.46 × 10^{-3} mg/mL by the fluorescent probe method (Figure 1a),

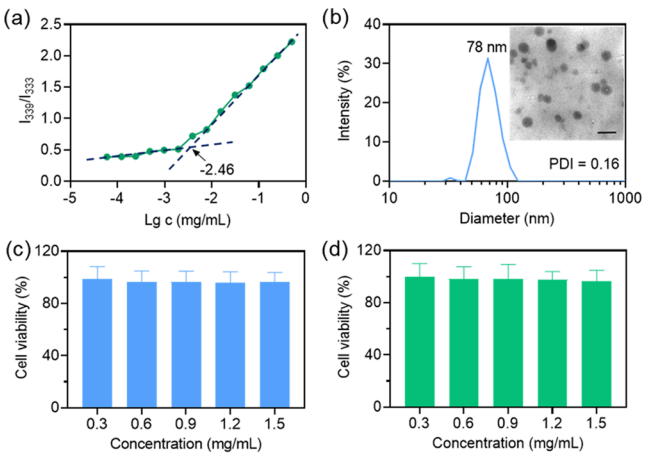

Figure 1. Characterization of PEG-PBnSec micelles. (a) Determination of the CMC of PEG-PBnSec with the fluorescent probe method. (b) Intensity-averaged size distribution and TEM image (inset) of PEG-PBnSec micelles in PBS (scale bar = 200 nm). Cytotoxicity of PEG-PBnSec micelles in HeLa (c) and H9C2 (d) cells following 48 h of incubation (n = 3).

which would enable the desired stability of the micelles against dilution. PEG-PBnSec micelles possessed a hydrodynamic diameter of 78 nm with a narrow size distribution (polydispersity index, PDI = 0.16), as determined by DLS. The TEM image revealed the spherical morphology of PEG-PBnSec micelles and consistent diameter to that measured by DLS (Figure 1b). Additionally, PEG-PBnSec micelles showed low cytotoxicity in HeLa and H9C2 cells, leading to cell viability over 90% at concentrations of up to 1.5 mg/mL (Figure 1c,d). These results collectively demonstrated that PEG-PBnSec micelles may serve as promising candidates as drug carriers.

ROS-Triggered Structural Change of PEG-PBnSec Micelles. Due to the larger atomic radius of selenium, polymers bearing selenoether groups show high sensitivity to ROS (0.1% H_2O_2) compared to those bearing thioether segments (10% H_2O_2).[29] To check the ROS sensitivity of PEG-PBnSec micelles, we studied their structural change in the presence of 0.1% H_2O_2. The side-chain selenoether groups could be oxidized into selenosulfones by H_2O_2 (Figure 2a), as

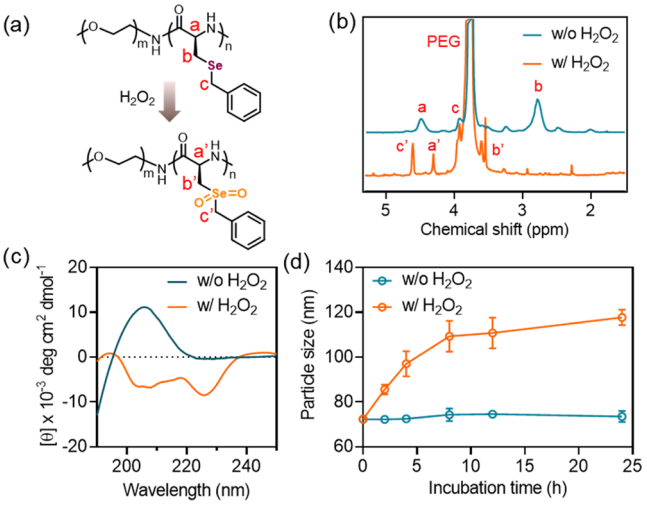

Figure 2. ROS-responsive structural change of PEG-PBnSec micelles. (a) Illustration of the chemical structure change of PEG-PBnSec after H_2O_2 treatment. ^{1}H NMR spectra of PEG-PBnSec (b), CD spectra of PEG-PBnSec (c), and particle size of PEG-PBnSec micelles (d) before and after treatment with 0.1% H_2O_2 (n = 3).

evidenced by the downfield shift of protons adjacent to selenoether groups in the ^{1}H NMR spectra (Figure 2b, from 2.8 and 3.9 to 3.6 and 4.6 ppm, respectively), mainly because of the stronger electron-withdrawing effect of the resulting selenosulfones. Moreover, the oxidation process did not cause degradation of the PEG-PBnSec (Figure S8), consistent with previous reports.[20,36] The enhanced polarity and hydrophilicity of selenosulfone groups triggered the conformational transition of the PBnSec segment, as evidenced by CD and FT-IR. Upon ROS treatment, a double minimum in the CD spectrum appeared at 206 and 225 nm (Figure 2c), and the characteristic amide I peak in the FT-IR spectrum shifted from 1632 to 1647 cm^{-1} (Figure S9). It therefore indicated the formation of an extended helical conformation as reported previously.[16,52,53] The conformational transition, together with the hydrophobic-to-hydrophilic change of the PBnSec segment, resulted in the destabilization of the PEG-PBnSec micelles. DLS analysis showed that the particle size of the micelles increased sharply after 2 h of treatment with H_2O_2 (0.1%) and plateaued at ∼109 nm after 8 h of incubation. Meanwhile, the PDI slightly increased when the incubation time was prolonged, suggesting the structural change of the micelles. On the contrary, the micelles maintained a relatively stable particle size (∼73 nm) after 24 h of incubation at 37 °C in the absence of H_2O_2 (Figure 2d and Table S1). The ROS-triggered structural transition did not significantly change the biocompatibility of the diblock copolymer, wherein the H_2O_2-treated PEG-PBnSec exhibited negligible toxicity in HeLa and H9C2 cell lines at concentrations of up to 1.5 mg/mL (Figure S10).

https://doi.org/10.1021/acs.biomac.2c00399
Biomacromolecules 2022, 23, 2647−2654

Drug Loading and *In Vitro* Drug Release from PEG-PBnSec/DOX Micelles. The drug-loaded micelles were prepared using DOX as a model chemotherapeutic agent, conferring the DLC of 21.3% and DLE of 75.2% as determined by spectrofluorimetry. The TEM image revealed the spherical structure of PEG-PBnSec/DOX micelles with an average diameter of ~67 nm (Figure 3a), and DLS analysis showed the hydrodynamic diameter of 73 nm (Figure 3c). The slightly smaller particle size of DOX-loaded micelles than that of blank micelles might be attributed to the hydrophobic interaction between DOX and the PBnSec segment that led to a more compact nanocore. After lyophilization of the DOX-loaded PEG-PBnSec micelles and resuspension in DI water, no micron-sized aggregates were observed, and the size of the micelles negligibly changed, mainly due to the presence of the PEG shell (Figure S11). Additionally, the DOX-loaded micelles maintained stability in PBS for up to 64 h, both in the presence and absence of 10% FBS (Figure S12). Nevertheless, after treatment with 0.1% H_2O_2 for 16 h, the particle size increased with a tendency to agglomerate, suggesting the structural change of the PEG-PBnSec/DOX micelles (Figure 3b,c).

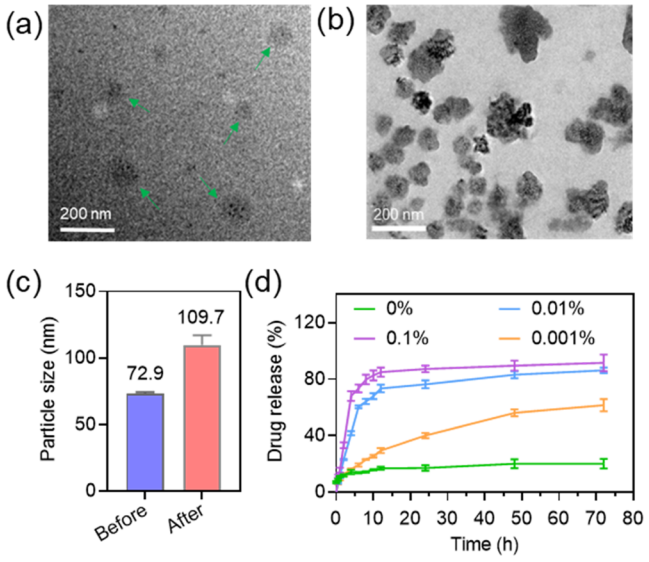

Figure 3. H_2O_2 responsiveness of DOX-loaded PEG-PBnSec micelles. TEM images of PEG-PBnSec/DOX micelles before (a) and after (b) 16 h of treatment with 0.1% H_2O_2. Green arrows point to micelles. (c) Size of PEG-PBnSec micelles before and after 16 h of treatment with 0.1% H_2O_2. (d) Cumulative release of DOX from PEG-PBnSec/DOX micelles in PBS (pH 7.4) with various H_2O_2 concentrations (n = 3).

Such ROS responsiveness encouraged us to further study the release of encapsulated DOX from PEG-PBnSec micelles upon H_2O_2 treatment. Micelles without H_2O_2 treatment exhibited a slow DOX release profile, reaching the accumulative release amount of 17.2% after 48 h of incubation (Figure 3d). In comparison, in the presence of 0.1% H_2O_2, the micelles exhibited a quick initial DOX release of 67.5% within the first 4 h and slowly reached equilibrium (82.6%) in the following 6 h. Such a result thus indicated the promoted DOX release as a consequence of H_2O_2-triggered micelles structural change. Interestingly, DOX can be effectively released from micelles at even lower H_2O_2 concentrations. For instance, about 68.2% of DOX was released after 10 h of treatment with 0.01% H_2O_2. When the H_2O_2 concentration was further decreased to 0.001%, the release rate was obviously slowed down, which nevertheless, was still faster than that in the absence of H_2O_2. As such, 61.5% of the encapsulated DOX could be released after 72 h of treatment with 0.001% H_2O_2. These results collectively indicated the high sensitivity of the selenopolypeptide-based micelles in triggered on-demand drug release.

***In Vitro* Antitumor Efficacy of PEG-PBnSec/DOX Micelles.** Considering the differences of the ROS level in tumor cells (usually up to 1×10^{-4} M) and normal cells (~2×10^{-8} M),[54,55] we went on to explore the selective release of encapsulated DOX from PEG-PBnSec micelles in cancer cells. As shown in Figure 4, the red fluorescence of DOX was clearly observed in the nuclei of all three tested tumor cell lines, including HeLa, HepG2, and 4T1 cells, indicating the H_2O_2-triggered dissociation of micelles and liberation of DOX that entered the nuclei and intercalated into DNA to emit

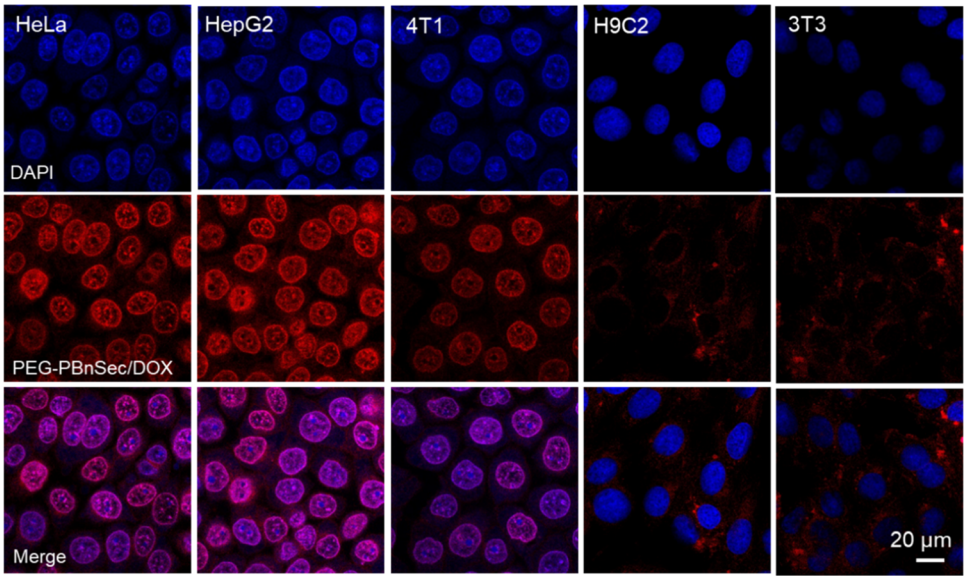

Figure 4. CLSM images of various cells after treatment with PEG-PBnSec/DOX micelles (20 μg/mL) for 12 h. Cell nuclei were stained with DAPI.

https://doi.org/10.1021/acs.biomac.2c00399
Biomacromolecules 2022, 23, 2647−2654

fluorescence. In contrast, weak red fluorescence was distributed in the cytoplasm of H9C2 and 3T3 cells, and minimal distribution was noted in the nuclei, which was attributed to the low ROS level in normal cells that are insufficient to dissociate the micelles, resulting in aggregation-induced fluorescence quenching of the encapsulated DOX (Figures S13 and S14). In support of such observation, when normal cells (3T3) were treated with PEG-PBnSec/DOX micelles in the presence of 0.1% H_2O_2, extensive nucleus distribution of DOX (red fluorescence) was noted, indicating release of DOX from the micelles (Figure S15).

Finally, we explored the cytotoxicity of DOX-encapsulated micelles in the above-mentioned cancerous and noncancerous cell lines, with free DOX as the control. In all three tumor cell lines, DOX-loaded micelles showed similar toxicities to free DOX in a concentration-dependent manner, suggesting efficient destabilization of micelles and intracellular release of the drug cargo. The half-inhibitory concentration (IC_{50}) of DOX-loaded micelles was calculated to be 0.85, 1.12, and 0.95 μg/mL in HeLa, HepG2, and 4T1 cells, respectively, slightly higher than that of free DOX (Table 1). In sharp contrast, the viabilities of H9C2 and 3T3 cells treated with DOX-loaded PEG-PBnSec micelles were dramatically higher than those treated with free DOX. The IC_{50} values of PEG-PBnSec/DOX micelles were >20 μg/mL in these two cell lines, much higher than those of free DOX (Table 1). These results further demonstrated that PEG-PBnSec/DOX micelles could efficiently and selectively release DOX in tumor cells in response to overproduced ROS, thereby provoking pronounced anticancer efficacy yet low cytotoxicity to normal cells (Figure 5).

Table 1. IC_{50} of Free DOX and DOX-Loaded Micelles in Various Cell Lines

	free DOX	DOX-loaded micelles
cell lines	IC_{50} (μg/mL)	IC_{50} (μg/mL)
HeLa	0.70	0.85
HepG2	1.04	1.12
4T1	0.84	0.95
H9C2	1.22	>20
3T3	1.94	>20

CONCLUSIONS

In conclusion, we designed and synthesized an amphiphilic diblock copolymer bearing a selenoether polypeptide segment (PEG-PBnSec), which can form ROS-responsive micelles to encapsulate hydrophobic chemodrugs (such as DOX) and selectively release the drug payloads in tumor cells with overproduced ROS. The oxidation of selenoether could be achieved at a much lower H_2O_2 concentration than that required to oxidize the thioether groups, and the oxidation caused structural change of the selenopolypeptide segment from the hydrophobic and random coiled structure to a hydrophilic and extended helical structure, ultimately leading to the structural change of micelles and release of the encapsulated drugs with high ROS responsiveness. As a result, the DOX-loaded PEG-PBnSec micelles exhibited potent and selective cytotoxicity in tumor cells *in vitro*. This work not only enriches the design of stimuli-responsive polypeptides, but also provides a promising candidate for the biomedical application of selenium-containing polymers.

ASSOCIATED CONTENT

Supporting Information

The Supporting Information is available free of charge at https://pubs.acs.org/doi/10.1021/acs.biomac.2c00399.

Preparation and characterization of micelles, monitoring the progress of ring-opening polymerization, GPC, and particle size (PDF)

AUTHOR INFORMATION

Corresponding Authors

Hua Lu − *Beijing National Laboratory for Molecular Sciences, Center for Soft Matter Science and Engineering, Key Laboratory of Polymer Chemistry and Physics of Ministry of Education, College of Chemistry and Molecular Engineering, Peking University, Beijing 100871, China;* orcid.org/0000-0003-2180-3091; Email: chemhualu@pku.edu.cn

Lichen Yin − *Institute of Functional Nano & Soft Materials (FUNSOM), Jiangsu Key Laboratory for Carbon-Based*

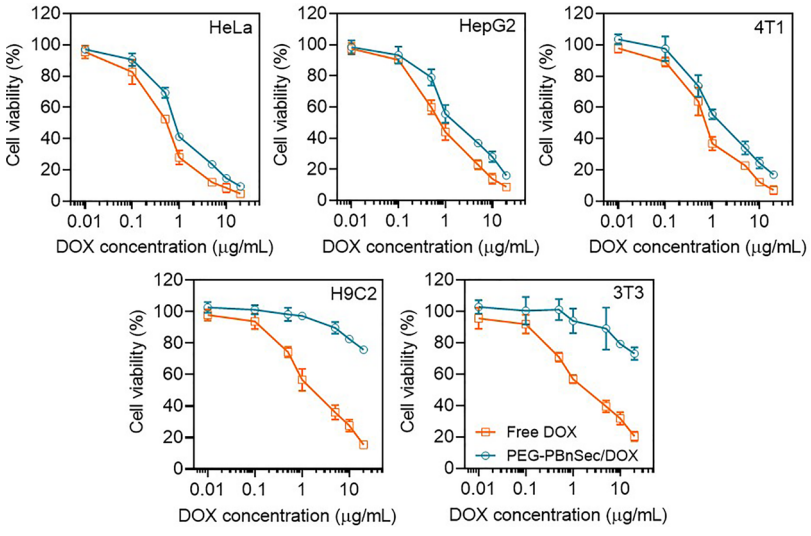

Figure 5. Cytotoxicity of PEG-PBnSec/DOX micelles at various DOX concentrations in different cell lines following 48 h of incubation (n = 3).

https://doi.org/10.1021/acs.biomac.2c00399
Biomacromolecules 2022, 23, 2647−2654

Functional Materials and Devices, Collaborative Innovation Center of Suzhou Nano Science & Technology, Soochow University, Suzhou 215123, China; orcid.org/0000-0002-4573-0555; Email: lcyin@suda.edu.cn

Authors

Chenglong Ge − *Institute of Functional Nano & Soft Materials (FUNSOM), Jiangsu Key Laboratory for Carbon-Based Functional Materials and Devices, Collaborative Innovation Center of Suzhou Nano Science & Technology, Soochow University, Suzhou 215123, China*

Junliang Zhu − *Institute of Functional Nano & Soft Materials (FUNSOM), Jiangsu Key Laboratory for Carbon-Based Functional Materials and Devices, Collaborative Innovation Center of Suzhou Nano Science & Technology, Soochow University, Suzhou 215123, China*

Guangqi Wu − *Beijing National Laboratory for Molecular Sciences, Center for Soft Matter Science and Engineering, Key Laboratory of Polymer Chemistry and Physics of Ministry of Education, College of Chemistry and Molecular Engineering, Peking University, Beijing 100871, China;* orcid.org/0000-0002-9763-6982

Huan Ye − *Institute of Functional Nano & Soft Materials (FUNSOM), Jiangsu Key Laboratory for Carbon-Based Functional Materials and Devices, Collaborative Innovation Center of Suzhou Nano Science & Technology, Soochow University, Suzhou 215123, China*

Complete contact information is available at: https://pubs.acs.org/10.1021/acs.biomac.2c00399

Author Contributions

§C.G. and J.Z. contributed equally.

Notes

The authors declare no competing financial interest.

■ ACKNOWLEDGMENTS

This work was supported by the National Natural Science Foundation of China (51873142), Suzhou Science and Technology Development Project (SYS2019072), 111 project, Suzhou Key Laboratory of Nanotechnology and Biomedicine, and Joint International Research Laboratory of Carbon-Based Functional Materials and Devices.

■ REFERENCES

(1) Deming, T. J. Synthetic Polypeptides for Biomedical Applications. *Prog. Polym. Sci.* **2007**, *32*, 858−875.
(2) Kwon, G. S.; Kataoka, K. Block Copolymer Micelles as Long-Circulating Drug Vehicles. *Adv. Drug Delivery Rev.* **2012**, *64*, 237−245.
(3) Deng, C.; Wu, J.; Cheng, R.; Meng, F.; Klok, H. A.; Zhong, Z. Functional Polypeptide and Hybrid Materials: Precision Synthesis via α-Amino Acid *N*-Carboxyanhydride Polymerization and Emerging Biomedical Applications. *Prog. Polym. Sci.* **2014**, *39*, 330−364.
(4) Song, Z.; Han, Z.; Lv, S.; Chen, C.; Chen, L.; Yin, L.; Cheng, J. Synthetic Polypeptides: From Polymer Design to Supramolecular Assembly and Biomedical Application. *Chem. Soc. Rev.* **2017**, *46*, 6570−6599.
(5) Melnyk, T.; Đorđević, S.; Conejos-Sánchez, I.; Vicent, M. J. Therapeutic Potential of Polypeptide-Based Conjugates: Rational Design and Analytical Tools That Can Boost Clinical Translation. *Adv. Drug Delivery Rev.* **2020**, *160*, 136−169.
(6) Rasines Mazo, A.; Allison-Logan, S.; Karimi, F.; Chan, N. J. A.; Qiu, W.; Duan, W.; O'Brien-Simpson, N. M.; Qiao, G. G. Ring Opening Polymerization of α-Amino Acids: Advances in Synthesis, Architecture and Applications of Polypeptides and Their Hybrids. *Chem. Soc. Rev.* **2020**, *49*, 4737−4834.
(7) Liu, Y.; Yin, L. α-Amino Acid *N*-Carboxyanhydride (NCA)-Derived Synthetic Polypeptides for Nucleic Acids Delivery. *Adv. Drug Delivery Rev.* **2021**, *171*, 139−163.
(8) Jiang, Y.; Chen, Y.; Song, Z.; Tan, Z.; Cheng, J. Recent Advances in Design of Antimicrobial Peptides and Polypeptides toward Clinical Translation. *Adv. Drug Delivery Rev.* **2021**, *170*, 261−280.
(9) Chen, Q.; Zhang, D.; Zhang, W.; Zhang, H.; Zou, J.; Chen, M.; Li, J.; Yuan, Y.; Liu, R. Dual Mechanism β-Amino Acid Polymers Promoting Cell Adhesion. *Nat. Commun.* **2021**, *12*, No. 562.
(10) Klemm, P.; Behnke, M.; Solomun, J. I.; Bonduelle, C.; Lecommandoux, S.; Traeger, A.; Schubert, S. Self-Assembled PEGylated Amphiphilic Polypeptides for Gene Transfection. *J. Mater. Chem. B* **2021**, *9*, 8224−8236.
(11) Zhang, P.; Cui, Y.; Anderson, C. F.; Zhang, C.; Li, Y.; Wang, R.; Cui, H. Peptide-Based Nanoprobes for Molecular Imaging and Disease Diagnostics. *Chem. Soc. Rev.* **2018**, *47*, 3490−3529.
(12) Shen, Y.; Fu, X.; Fu, W.; Li, Z. Biodegradable Stimuli-Responsive Polypeptide Materials Prepared by Ring Opening Polymerization. *Chem. Soc. Rev.* **2015**, *44*, 612−622.
(13) Zhang, P.; Li, M.; Xiao, C.; Chen, X. Stimuli-Responsive Polypeptides for Controlled Drug Delivery. *Chem. Commun.* **2021**, *57*, 9489−9503.
(14) Wang, X.; Song, Z.; Wei, S.; Ji, G.; Zheng, X.; Fu, Z.; Cheng, J. Polypeptide-Based Drug Delivery Systems for Programmed Release. *Biomaterials* **2021**, *275*, No. 120913.
(15) Song, Z.; Fu, H.; Wang, R.; Pacheco, L. A.; Wang, X.; Lin, Y.; Cheng, J. Secondary Structures in Synthetic Polypeptides from *N*-Carboxyanhydrides: Design, Modulation, Association, and Material Applications. *Chem. Soc. Rev.* **2018**, *47*, 7401−7425.
(16) Bonduelle, C. Secondary Structures of Synthetic Polypeptide Polymers. *Polym. Chem.* **2018**, *9*, 1517−1529.
(17) Ge, C.; Ye, H.; Wu, F.; Zhu, J.; Song, Z.; Liu, Y.; Yin, L. Biological Applications of Water-Soluble Polypeptides with Ordered Secondary Structures. *J. Mater. Chem. B* **2020**, *8*, 6530−6547.
(18) Zhou, Z.; Shen, Y.; Tang, J.; Fan, M.; Van Kirk, E. A.; Murdoch, W. J.; Radosz, M. Charge-Reversal Drug Conjugate for Targeted Cancer Cell Nuclear Drug Delivery. *Adv. Funct. Mater.* **2009**, *19*, 3580−3589.
(19) Takemoto, H.; Ishii, A.; Miyata, K.; Nakanishi, M.; Oba, M.; Ishii, T.; Yamasaki, Y.; Nishiyama, N.; Kataoka, K. Polyion Complex Stability and Gene Silencing Efficiency with a siRNA-Grafted Polymer Delivery System. *Biomaterials* **2010**, *31*, 8097−8105.
(20) Kramer, J. R.; Deming, T. J. Glycopolypeptides with a Redox-Triggered Helix-to-Coil Transition. *J. Am. Chem. Soc.* **2012**, *134*, 4112−4115.
(21) Sulistio, A.; Blencowe, A.; Widjaya, A.; Zhang, X.; Qiao, G. Development of Functional Amino Acid-Based Star Polymers. *Polym. Chem.* **2012**, *3*, 224−234.
(22) Petitdemange, R.; Garanger, E.; Bataille, L.; Dieryck, W.; Bathany, K.; Garbay, B.; Deming, T. J.; Lecommandoux, S. Selective Tuning of Elastin-like Polypeptide Properties via Methionine Oxidation. *Biomacromolecules* **2017**, *18*, 544−550.
(23) Chen, J.; Ding, J.; Xu, W.; Sun, T.; Xiao, H.; Zhuang, X.; Chen, X. Receptor and Microenvironment Dual-Recognizable Nanogel for Targeted Chemotherapy of Highly Metastatic Malignancy. *Nano Lett.* **2017**, *17*, 4526−4533.
(24) Teng, W.; Jia, F.; Han, H.; Qin, Z.; Jin, Q.; Ji, J. Polyamino Acid-Based Gemcitabine Nanocarriers for Targeted Intracellular Drug Delivery. *Polym. Chem.* **2017**, *8*, 2490−2498.
(25) Deming, T. J. Functional Modification of Thioether Groups in Peptides, Polypeptides, and Proteins. *Bioconjugate Chem.* **2017**, *28*, 691−700.
(26) Fu, X.; Ma, Y.; Shen, Y.; Shen, Y.; Fu, W.; Fu, W.; Li, Z. Oxidation-Responsive OEGylated Poly-$_L$-cysteine and Solution Properties Studies. *Biomacromolecules* **2014**, *15*, 1055−1061.
(27) Liu, G.; Zhou, L.; Guan, Y.; Su, Y.; Dong, C. M. Multi-Responsive Polypeptidosome: Characterization, Morphology Trans-

formation, and Triggered Drug Delivery. *Macromol. Rapid Commun.* **2014**, *35*, 1673−1678.
(28) Qian, C.; Feng, P.; Yu, J.; Chen, Y.; Hu, Q.; Sun, W.; Xiao, X.; Hu, X.; Bellotti, A.; Shen, Q. D.; Gu, Z. Anaerobe-Inspired Anticancer Nanovesicles. *Angew. Chem. Int. Ed.* **2017**, *56*, 2588−2593.
(29) Liu, H.; Wang, R.; Wei, J.; Cheng, C.; Zheng, Y.; Pan, Y.; He, X.; Ding, M.; Tan, H.; Fu, Q. Conformation-Directed Micelle-to-Vesicle Transition of Cholesterol-Decorated Polypeptide Triggered by Oxidation. *J. Am. Chem. Soc.* **2018**, *140*, 6604−6610.
(30) Zheng, Y.; Wang, Z.; Li, Z.; Liu, H.; Wei, J.; Peng, C.; Zhou, Y.; Li, J.; Fu, Q.; Tan, H.; Ding, M. Ordered Conformation-Regulated Vesicular Membrane Permeability. *Angew. Chem. Int. Ed.* **2021**, *60*, 22529−22536.
(31) Fan, Z.; Xu, H. Recent Progress in the Biological Applications of Reactive Oxygen Species-Responsive Polymers. *Polym. Rev.* **2020**, *60*, 114−143.
(32) Huang, X.; Liu, X.; Luo, Q.; Liu, J.; Shen, J. Artificial Selenoenzymes: Designed and Redesigned. *Chem. Soc. Rev.* **2011**, *40*, 1171−1184.
(33) Xia, J.; Li, T.; Lu, C.; Xu, H. Selenium-Containing Polymers: Perspectives toward Diverse Applications in Both Adaptive and Biomedical Materials. *Macromolecules* **2018**, *51*, 7435−7455.
(34) Xu, H.; Cao, W.; Zhang, X. Selenium-Containing Polymers: Promising Biomaterials for Controlled Release and Enzyme Mimics. *Acc. Chem. Res.* **2013**, *46*, 1647−1658.
(35) Cao, Z.; Li, D.; Wang, J.; Yang, X. Reactive Oxygen Species-Sensitive Polymeric Nanocarriers for Synergistic Cancer Therapy. *Acta Biomater.* **2021**, *130*, 17−31.
(36) Ma, N.; Li, Y.; Ren, H.; Xu, H.; Li, Z.; Zhang, X. Selenium-Containing Block Copolymers and Their Oxidation-Responsive Aggregates. *Polym. Chem.* **2010**, *1*, 1609−1614.
(37) Miao, X.; Cao, W.; Zheng, W.; Wang, J.; Zhang, X.; Gao, J.; Yang, C.; Kong, D.; Xu, H.; Wang, L.; Yang, Z. Switchable Catalytic Activity: Selenium-Containing Peptides with Redox-Controllable Self-Assembly Properties. *Angew. Chem. Int. Ed.* **2013**, *52*, 7781−7785.
(38) Liu, J.; Pang, Y.; Zhu, Z.; Wang, D.; Li, C.; Huang, W.; Zhu, X.; Yan, D. Therapeutic Nanocarriers with Hydrogen Peroxide-Triggered Drug Release for Cancer Treatment. *Biomacromolecules* **2013**, *14*, 1627−1636.
(39) Li, T.; Xu, H. Selenium-Containing Nanomaterials for Cancer Treatment. *Cell Rep. Phys. Sci.* **2020**, *1*, No. 100111.
(40) Huang, Y.; Su, E.; Ren, J.; Qu, X. The Recent Biological Applications of Selenium-Based Nanomaterials. *Nano Today* **2021**, *38*, No. 101205.
(41) Pan, S.; Li, T.; Tan, Y.; Xu, H. Selenium-containing Nanoparticles Synergistically Enhance Pemetrexed&NK Cell-based Chemoimmunotherapy. *Biomaterials* **2022**, *280*, No. 121321.
(42) Wu, G.; Ge, C.; Liu, X.; Wang, S.; Wang, L.; Yin, L.; Lu, H. Synthesis of Water Soluble and Multi-Responsive Selenopolypeptides via Ring-Opening Polymerization of *N*-Carboxyanhydrides. *Chem. Commun.* **2019**, *55*, 7860−7863.
(43) Yao, Q.; Wu, G.; Hao, H.; Lu, H.; Gao, Y. Redox-Mediated Reversible Supramolecular Assemblies Driven by Switch and Interplay of Peptide Secondary Structures. *Biomacromolecules* **2021**, *22*, 2563−2572.
(44) Dong, C.; Wu, G.; Chen, C.; Li, X.; Yuan, R.; Xu, L.; Guo, H.; Zhang, J.; Lu, H.; Wang, F. Site-Specific Conjugation of a Selenopolypeptide to Alpha-1-antitrypsin Enhances Oxidation Resistance and Pharmacological Properties. *Angew. Chem. Int. Ed.* **2022**, *61*, No. e202115241.
(45) Lv, S.; Wu, Y.; Cai, K.; He, H.; Li, Y.; Lan, M.; Chen, X.; Cheng, J.; Yin, L. High Drug Loading and Sub-Quantitative Loading Efficiency of Polymeric Micelles Driven by Donor-Receptor Coordination Interactions. *J. Am. Chem. Soc.* **2018**, *140*, 1235−1238.
(46) Wu, Y.; Lv, S.; Li, Y.; He, H.; Ji, Y.; Zheng, M.; Liu, Y.; Yin, L. Co-Delivery of Dual Chemo-Drugs with Precisely Controlled, High Drug Loading Polymeric Micelles for Synergistic Anti-Cancer Therapy. *Biomater. Sci.* **2020**, *8*, 949−959.
(47) Shi, X.; Zhang, Y.; Tian, Y.; Xu, S.; Ren, E.; Bai, S.; Chen, X.; Chu, C.; Xu, Z.; Liu, G. Multi-Responsive Bottlebrush-Like Unimolecules Self-Assembled Nano-Riceball for Synergistic Sono-Chemotherapy. *Small Methods* **2021**, *5*, No. 2000416.
(48) Wang, M.; Han, L.; Zhu, Y.; Qi, R.; Tian, L.; He, F. Formation of Hierarchical Architectures with Dimensional and Morphological Control in the Self-Assembly of Conjugated Block Copolymers. *Small Methods* **2020**, *4*, No. 1900470.
(49) Liu, X.; Zhao, Z.; Wu, F.; Chen, Y.; Yin, L. Tailoring Hyperbranched Poly(*β*-Amino Ester) as a Robust and Universal Platform for Cytosolic Protein Delivery. *Adv. Mater.* **2022**, *34*, No. 2108116.
(50) Hou, M.; Wu, X.; Zhao, Z.; Deng, Q.; Chen, Y.; Yin, L. Endothelial Cell-Targeting, ROS-Ultrasensitive Drug/siRNA Co-Delivery Nanocomplexes Mitigate Early-Stage Neutrophil Recruitment for the Anti-Inflammatory Treatment of Myocardial Ischemia Reperfusion Injury. *Acta Biomater.* **2022**, *143*, 344−355.
(51) Gao, L.; Cheng, J.; Shen, Z.; Zhang, G.; Liu, S.; Hu, J. Orchestrating Nitric Oxide and Carbon Monoxide Signaling Molecules for Synergistic Treatment of MRSA Infections. *Angew. Chem. Int. Ed.* **2022**, *61*, No. e202112782.
(52) Kramer, J. R.; Onoa, B.; Bustamante, C.; Bertozzi, C. R. Chemically Tunable Mucin Chimeras Assembled on Living Cells. *Proc. Natl. Acad. Sci. U.S.A.* **2015**, *112*, 12574−12579.
(53) Benavides, I.; Raftery, E. D.; Bell, A. G.; Evans, D.; Scott, W. A.; Houk, K. N.; Deming, T. J. Poly(dehydroalanine): Synthesis, Properties, and Functional Diversification of a Fluorescent Polypeptide. *J. Am. Chem. Soc.* **2022**, *144*, 4214−4223.
(54) Ye, H.; Zhou, Y.; Liu, X.; Chen, Y.; Duan, S.; Zhu, R.; Liu, Y.; Yin, L. Recent Advances on Reactive Oxygen Species Responsive Delivery and Diagnosis System. *Biomacromolecules* **2019**, *20*, 2441−2463.
(55) Jing, X.; Hu, H.; Sun, Y.; Yu, B.; Cong, H.; Shen, Y. The Intracellular and Extracellular Microenvironment of Tumor Site: The Trigger of Stimuli-Responsive Drug Delivery Systems. *Small Methods* **2022**, *6*, No. 2101437.

https://doi.org/10.1021/acs.biomac.2c00399
Biomacromolecules 2022, 23, 2647−2654